

Yujiong Liu

Robotics and Mechatronics Laboratory,
Department of Mechanical Engineering,
Virginia Polytechnic Institute
and State University,
Blacksburg, VA 24060
e-mail: yjliu@vt.edu

Minxiu Kong

Robotics Institute School of
Mechatronics Engineering,
Harbin Institute of Technology,
Harbin 150001, China
e-mail: exk@hit.edu.cn

Neng Wan

Advanced Controls Research Laboratory,
Department of Mechanical Science
and Engineering,
University of Illinois at Urbana-Champaign,
Urbana, IL 61801
e-mail: nengwan2@illinois.edu

Pinhas Ben-Tzvi¹

Mem. ASME
Robotics and Mechatronics Laboratory,
Department of Mechanical Engineering,
Virginia Polytechnic Institute
and State University,
Blacksburg, VA 24060
e-mail: bentzvi@vt.edu

A Geometric Approach to Obtain the Closed-Form Forward Kinematics of H4 Parallel Robot

To obtain the closed-form forward kinematics of parallel robots, researchers use algebra-based method to transform and simplify the constraint equations. However, this method requires a complicated derivation that leads to high-order univariate variable equations. In fact, some particular mechanisms, such as Delta, or H4 possess many invariant geometric properties during movement. This suggests that one might be able to transform and reduce the problem using geometric approaches. Therefore, a simpler and more efficient solution might be found. Based on this idea, we developed a new geometric approach called geometric forward kinematics (GFK) to obtain the closed-form solutions of H4 forward kinematics in this paper. The result shows that the forward kinematics of H4 yields an eighth degree univariate polynomial, compared with earlier reported 16th degree. Thanks to its clear physical meaning, an intensive discussion about the solutions is presented. Results indicate that a general H4 robot can have up to eight nonrepeated real solutions for its forward kinematics. For a specific configuration of H4, the non-repeated number of real roots could be restricted to only two, four, or six. Two traveling plate configurations are discussed in this paper as two typical categories of H4. A numerical analysis was also performed for this new method. [DOI: 10.1115/1.4040703]

1 Introduction

For the study of parallel robots, one of the fundamental problems is to compute the forward and inverse kinematics. However, compared to serial robots, the forward kinematics of parallel robots is a challenging problem due to the difficulties of deriving closed-form solutions.

To address these challenges, researchers have proposed various methods that can be generally classified into three types: (1) numerical convergence methods, (2) algebra-based methods, and (3) geometry-based methods. The classical numerical method uses Newton iteration scheme [1] or its variants to solve the constraint equations although other methods [2] were also considered. This method is the most popular approach due to its simplified programming and lower computational time. Usually, researchers using this approach are more concerned with the computational efficiency. Therefore, they prefer to develop specific algorithms for specific mechanisms in order to optimize the performance. For instance, a new approach for Gough–Stewart platform is based on multibody formulation [3] and a fast computation algorithm for cable-driven parallel mechanisms [4]. Another emerging method for numerical computation is interval analysis which was introduced by Merlet [5].

The algebra-based method utilizes an algebraic means to solve the constraint equations. The basic idea of this method involves transforming the constraint equations to linear forms by introducing intermediate variables. This method is used by most

researchers to obtain analytical forward kinematics solutions like in the Gough–Stewart platform [6–9] and a class of four degree-of-freedom (DOF) parallel mechanisms [10].

Geometry-based method is an alternative means to derive the closed-form forward kinematics solutions. The basic idea of this method is to use the geometric properties of the specific mechanisms to transform and reduce the problem, and then use the analytical geometric means to finally obtain the solutions. A typical example is the forward kinematics solution of DELTA [11]. By translating the forearms to the center of the traveling plate, the forward kinematics can be reduced to a simpler geometric problem, which involves finding the center from three known points on a sphere. Other successful applications of the geometric approach include a casing oscillator [12] and a special Stewart platform [13].

Compared with algebraic method, geometric methods have several drawbacks. First, they are all heavily dependent on the properties of the specific mechanism, like the pure translation of the DELTA. Second, because of the first point, they usually cannot be adopted for other mechanisms. However, they also have some irreplaceable advantages, including easy derivations and the clear physical meanings of the variables during derivation. These advantages simplify the postprocessing of the solution (i.e., choosing the valid root of the final equation), thus decreasing the overall computation time.

It is worth noting that modern research on mechanisms tends to use modern mathematical tools due to their insightful descriptions of rigid body motion, such as the approaches based on screw theory [14], Lie groups [15], or dual quaternions [16]. These approaches represent new methods to establish the equations. However, solving these equations in practice relies on either numerical methods or algebraic manipulation. Therefore, these

¹Corresponding author.

Contributed by the Mechanisms and Robotics Committee of ASME for publication in the JOURNAL OF MECHANISMS AND ROBOTICS. Manuscript received March 16, 2018; final manuscript received June 22, 2018; published online July 18, 2018. Assoc. Editor: Damien Chablat.

approaches can still be categorized as numerical or algebraic approaches.

Compared with the common 6DOF and 3DOF parallel robots, H4 [17] is a new class of 4DOF parallel robots developed by Pierrot in 2001. Due to its additional rotational DOF introduced by the articulated traveling plate, H4 has a much more difficult forward kinematics compared with the Delta robot, especially for the closed form solution. To date, the most widely used approach to address this problem is based on numerical iteration [17]. However, since this method is developed under practical considerations and the iterative formula is not in closed form, the numerical approach is not suitable for handling further mechanism analysis. In addition, a closed form solution is usually preferable due to the guaranteed maximum computation time and the lack of local maximum. Therefore, Choi et al. formulated a closed form solution based on algebraic manipulations of the constraint equations [18]. Their work shows that the H4 forward kinematics yields a 16th degree univariate polynomial. However, due to the complexity and lack of physical meaning of the algebraic approach, they did not discuss the real roots of the polynomial, as stated by the H4 inventors Pierrot et al. [19] that no further research has been carried out regarding the forward kinematic problem (FKP), such as the number of real roots of the polynomial. This motivates our work to develop a new FKP solution with geometrically interpretable variables as well as in closed form so that it can be used to further analyze the H4 mechanism.

In this paper, we propose a geometric approach to solve the forward kinematic problem of H4 mechanism, which treats the two chains that are connected to the same lateral bar as one group. Therefore, the translation step can be proceeded inside the groups separately without being affected by the rotational DOF. After this reduction, the original problem becomes a simplified geometric problem, which can be handled easily by analytical geometry. Due to this geometric approach employed, this method is referred to as for the geometric forward kinematics (GFK).

The scope of this paper is to present a new method to obtain the closed-form forward kinematics solutions of 4DOF H4 parallel robots. After brief description of the H4 concept, a geometric model is established. Then, the specific steps to transform and reduce this geometric model are presented. Since different traveling plate structures affect the formulation of the forward kinematics, the articulated case and the prismatic case are discussed separately. Following these, the main work focuses on the analytical geometric derivation. In addition, the root analysis and the numerical robustness of the GFK are discussed at the end of this paper.

It is worth to note that, in this paper, H4 represents one class of 4DOF parallel robots, while Par4 [19], I4 [20], I4R [21], and Heli4 [22] are the four practical implementations of the general H4 concept appeared in the literature. There are other configurations for the H4 mechanism, for instance, the asymmetric designs that appeared in Ref. [23] and those using prismatic actuators [17]. Based on the geometric derivations of this paper, all the H4 robots with articulated traveling plate structures have the same FKP solutions. Similarly, all H4 robots with prismatic traveling plate structures have the same FKP solutions. Therefore, for a specific H4 robot, the forward kinematic problem can be solved by applying one of the two cases developed in this paper based on its corresponding traveling plate structure. However, Heli4 is an exception to this categorization, which utilizes a helical traveling plate structure. Since its inventors have already applied the geometric approach [22] to obtain the forward kinematics, this case is not discussed in this paper.

2 Derivation of the Geometric Forward Kinematics

As shown in Fig. 1, a typical H4 parallel mechanism consists of four P/R-U-U chains and two revolute joints. The four chains can be treated as two groups because they are connected to two different lateral bars. The two chains together with the connected lateral

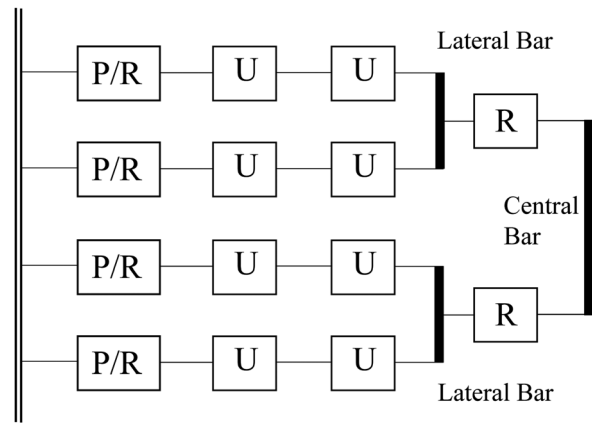


Fig. 1 A typical H4 configuration: the first two P/R-U-U chains connect to the first lateral bar. The third and fourth chain connects to the second lateral bar. The two lateral bars are connected to the central bar by two revolute joints.

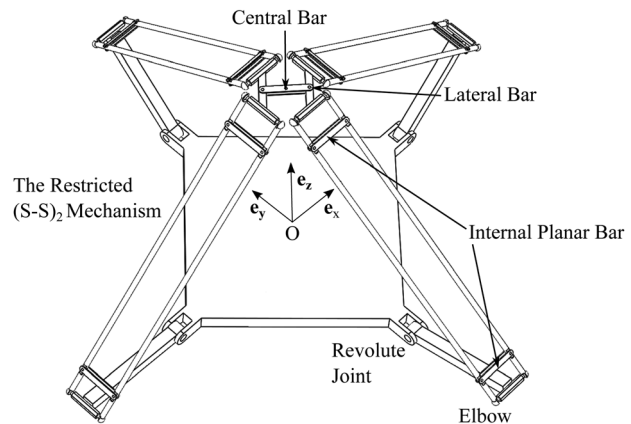


Fig. 2 One practical H4 kinematics configuration. In this configuration, the U-U chain is replaced by a restricted (S-S)₂ mechanism and the four chains are designed to have identical properties.

bar constitute a relatively independent submechanism. This submechanism is able to conduct three translational DOFs. Then, the two submechanisms are connected to a central bar by two revolute joints. The central bar is the so-called traveling plate. Figure 2 shows more details of a practical H4 kinematic configuration.

Among all the good kinematics properties of H4, two insightful observations are important to our geometric transformation and reduction process listed as follows: (1) the lateral bar connected by two P/R-U-U chains can only translate and (2) the central bar constrains the two lateral bars in the same plane.

The H4 concept can be implemented in several configurations in practice, such as Par4 and I4. Par4 is a symmetric H4 with four identical (S-S)₂ chains (or (U-S)₂ chains to avoid the internal DOF for each rod) and four symmetrically arranged actuators. To avoid internal singularity [24], the traveling plate of Par4 is designed to form a planar parallelogram, as shown in Fig. 3. Figure 2 shows another practical configuration of H4, where the U-U connection is replaced by a restricted (S-S)₂ pair (the twist DOF of the (S-S)₂ pair is restricted by two internal planar bars). This forces the restricted (S-S)₂ pair to behave like a planar parallelogram, which ensures the pure translation of the lateral bars. Note that the H4 robot in Fig. 2 is designed to illustrate the forward kinematics for the articulated traveling plate case. The internal singularity, stiffness, and other kinematic related issues are

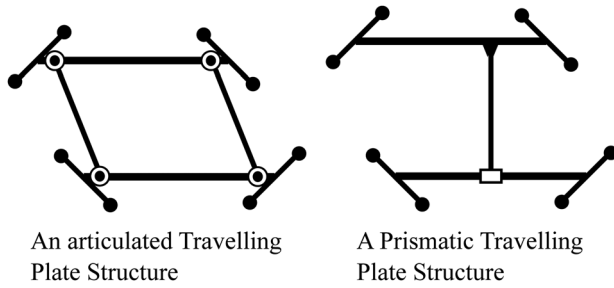


Fig. 3 Two typical traveling plate structures of the H4 robots. Left belongs to Par4 and the right belongs to I4.

not considered here. I4 is another well-known H4 robot whose articulated traveling plate is replaced by a prismatic structure, as shown in Fig. 3.

2.1 Geometric Transformation and Reduction. The forward kinematics procedure for a parallel mechanism involves the computation of the position and orientation of the traveling plate, given the independent joint angles. However, since H4 has many different kinematic configurations and our goal is to cover all the situations, we do not derive our formulas directly from the joint angles. Instead, we assume that the elbow positions are given. This is a reasonable assumption because it is simple to compute the elbow positions from the joint angles. Based on this setting, the forward kinematics of the H4 can be described as a geometric problem.

Problem: As shown in Fig. 4, four known points are described: $B_1, B_2, B_3,$ and B_4 , which represent the known elbow positions. The distances from these four points to the corresponding lateral bar vertices $C_1, C_2, C_3,$ and C_4 are known. The vectors C_1C_2 and C_4C_3 are known. The traveling plate structure is known. Find the position of the central bar.

From the given conditions, the vector C_1C_2 is constant, which means that the lateral bars cannot change their directions during movement. This observation allows us to translate the four sides B_iC_i along C_1C_2 without changing the position of the central bar. Therefore, side B_1C_1 is moved from C_1 to D_1 , and side B_2C_2 is moved from C_2 to D_1 . Likewise, B_3C_3 is moved from C_3 to D_2 and B_4C_4 is moved from C_4 to D_2 . D_1 and D_2 are the centers of the lateral bars. This step is shown in Fig. 5. After this simplification, the points C_i and the vector C_1C_2 are eliminated. Their information is combined into the new points $B'_1, B'_2, B'_3,$ and B'_4 . Thus, the original problem becomes:

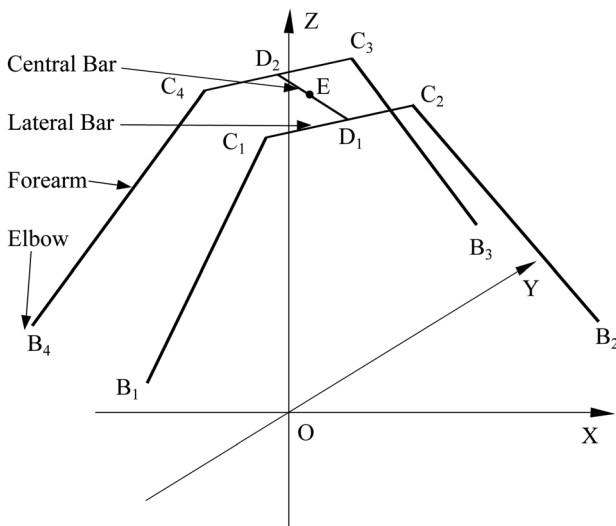


Fig. 4 Geometric model of the H4 forward kinematics

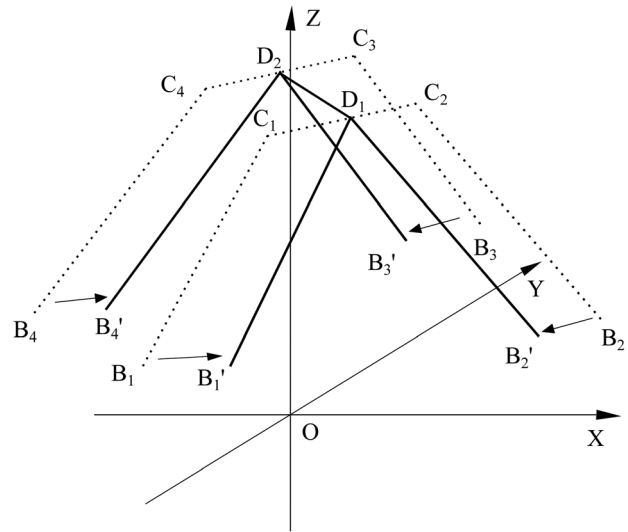


Fig. 5 Simplification of the original geometric problem: since the lateral bars keep their direction during movement, each side B_iC_i is translated from C_i to the corresponding lateral bar center

Problem: There are four known points: $B'_1, B'_2, B'_3,$ and B'_4 . The distances from these four points to the corresponding lateral bar centers D_1 and D_2 are known. The constraint between D_1 and D_2 is known. Find the position of the central bar.

It can be easily found that the set of D_1 and D_2 is two circles whose centers and radiuses can be obtained by computing the triangles $\triangle B'_1B'_2D_1$ and $\triangle B'_3B'_4D_2$. Therefore, the second step is to utilize the constraint between D_1 and D_2 to connect these two circles, and finally, solve the problem. For this step, as different H4 versions have different constraints between D_1 and D_2 , there are two situations that need to be discussed.

2.2 Forward Kinematics of the Articulated Traveling Plate. An articulated traveling plate uses revolute joints to connect the lateral bars and the central bar. Therefore, the constraints between D_1 and D_2 are as follows: (a) D_1D_2 stays in the horizontal plane, i.e., $D_1D_2 \cdot [001]^T = 0$; and (b) $\|D_1D_2\| = e$, where e is the length of the central bar.

Adding these two conditions to the reduced problem above and using the analytical geometry method, one set of constraint equations can be obtained. By handling these equations, the closed-form solutions can be obtained. To make this specific derivation clear, we divide it into the following two main steps:

Step 1: Obtain the constraint equations

Referring to Figs. 5 and 6, from the four spatial points B_i ($i=1,2,3,4$ is the index of each chain) and lateral bar vector $\mathbf{u} = [u_x u_y u_z]^T = C_1C_2$, we can get the four new elbow position vectors OB'_i

$$OB'_i = OB_i + c_i \mathbf{u} \quad (1)$$

where c_i is the i th entry of the coefficient matrix $\mathbf{c} = [0.5 \ -0.5 \ -0.5 \ 0.5]$. And the position vector $OO_j = [o_{x,j} \ o_{y,j} \ o_{z,j}]^T$ of the center O_j , the normal vector $\mathbf{n}_j = [n_{x,j} \ n_{y,j} \ n_{z,j}]^T$, and the radius r_j of circle Cir_j ($j=1, 2$ is the index of the two parametrized circles) are given by

$$\begin{aligned} OO_j &= (OB'_{2j-1} + OB'_{2j})/2 \\ \mathbf{n}_1 &= OB'_2 - OB'_1 \\ \mathbf{n}_2 &= OB'_3 - OB'_4 \\ r_j &= \sqrt{c^2 - \mathbf{n}_j^T \mathbf{n}_j} / 4 \end{aligned} \quad (2)$$

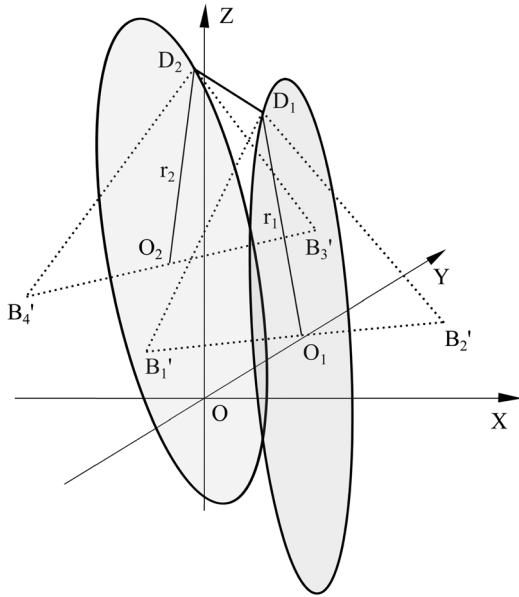


Fig. 6 For the case of an articulated traveling plate, the constraints between D_1 and D_2 are $\|D_1D_2\| = e$ and $D_1D_2 \cdot [0\ 0\ 1]^T = 0$. The circles with centers O_1 and O_2 are the possible positions for D_1 and D_2 , respectively, before adding D_1D_2 constraints.

where c is the length of the forearm. Therefore, the parametric equation of Cir_j can be obtained as follows:

$$\mathbf{p}_1 = \mathbf{K}_1 \cdot [\cos \alpha \quad \sin \alpha \quad 1]^T \quad (3)$$

$$\mathbf{p}_2 = \mathbf{K}_2 \cdot [\cos \beta \quad \sin \beta \quad 1]^T \quad (4)$$

where $\mathbf{p}_j = [x_j \ y_j \ z_j]^T$ is the position vector of an arbitrary point on Cir_j , and α and β are the parameterized variables for Cir_1 and Cir_2 , respectively. The coefficient matrices \mathbf{K}_1 and \mathbf{K}_2 are given by

$$\mathbf{K}_j = \begin{bmatrix} r_j \cos \gamma_j & 0 & o_{x,j} \\ r_j \sin \theta_j \sin \gamma_j & r_j \cos \theta_j & o_{y,j} \\ -r_j \cos \theta_j \sin \gamma_j & r_j \sin \theta_j & o_{z,j} \end{bmatrix}$$

where

$$\begin{aligned} \sin \gamma_j &= n_{x,j} / \|\mathbf{n}_j\| \\ \cos \gamma_j &= \sqrt{\mathbf{n}_j^T \mathbf{n}_j - n_{x,j}^2} / \|\mathbf{n}_j\| \\ \sin \theta_j &= -n_{y,j} / \sqrt{\mathbf{n}_j^T \mathbf{n}_j - n_{x,j}^2} \\ \cos \theta_j &= n_{z,j} / \sqrt{\mathbf{n}_j^T \mathbf{n}_j - n_{x,j}^2} \end{aligned}$$

Finally, by setting $z_1 = z_2$ and $\|D_1D_2\| = e$, we establish the constraint equations

$$\begin{cases} k_{31,1} \cos \alpha + k_{32,1} \sin \alpha + k_{33,1} \\ = k_{31,2} \cos \beta + k_{32,2} \sin \beta + k_{33,2} \end{cases} \quad (5)$$

$$(x_1 - x_2)^2 + (y_1 - y_2)^2 = e^2 \quad (6)$$

where $k_{pq,j}$ is the entry of matrix \mathbf{K}_j in the p th row and the q th column. Note that there are only two unknown variables in Eqs. (5) and (6), which are much simpler to solve for than the algebra-based method.

Step 2: Solve the constraint equations

At first, we use the substitution method to simplify Eq. (5). Let

$$\begin{aligned} \sin t_\alpha &= k_{31,1}/s_1 & \cos t_\alpha &= k_{32,1}/s_1 \\ \sin t_\beta &= k_{31,2}/s_2 & \cos t_\beta &= k_{32,2}/s_2 \end{aligned}$$

where

$$s_j = \sqrt{k_{31,j}^2 + k_{32,j}^2}$$

Then, Eq. (5) can be transformed into

$$s_1 \sin(\alpha + t_\alpha) + k_{33,1} = s_2 \sin(\beta + t_\beta) + k_{33,2} \quad (7)$$

By denoting

$$\begin{aligned} \alpha' &= \alpha + t_\alpha & p_{11} &= s_1/s_2 \\ \beta' &= \beta + t_\beta & p_{12} &= (k_{33,1} - k_{33,2})/s_2 \end{aligned}$$

Equation (7) can be written as

$$p_{11} \sin \alpha' + p_{12} = \sin \beta' \quad (8)$$

As for Eq. (6), substitute corresponding x_i and y_i from Eqs. (3) and (4) into Eq. (6) and use α' and β' as the new unknowns (use the relations $\alpha = \alpha' - t_\alpha$ and $\beta = \beta' - t_\beta$). This yields

$$\begin{aligned} &(p_{21} \cos \alpha' + p_{22} \sin \alpha' + p_{23} \cos \beta' + p_{24})^2 \\ &+ (p_{25} \cos \alpha' + p_{26} \sin \alpha' + p_{27} \cos \beta' + p_{28})^2 = e^2 \end{aligned} \quad (9)$$

where its coefficients can be precomputed as follows:

$$\begin{aligned} p_{21} &= k_{11,1} \cos t_\alpha - k_{12,1} \sin t_\alpha \\ p_{22} &= k_{11,1} \sin t_\alpha + k_{12,1} \cos t_\alpha - (k_{11,2} \sin t_\beta + k_{12,2} \cos t_\beta)p_{11} \\ p_{23} &= -k_{11,2} \cos t_\beta + k_{12,2} \sin t_\beta \\ p_{24} &= k_{13,1} - k_{13,2} - (k_{11,2} \sin t_\beta + k_{12,2} \cos t_\beta)p_{12} \\ p_{25} &= k_{21,1} \cos t_\alpha - k_{22,1} \sin t_\alpha \\ p_{26} &= k_{21,1} \sin t_\alpha + k_{22,1} \cos t_\alpha - (k_{21,2} \sin t_\beta + k_{22,2} \cos t_\beta)p_{11} \\ p_{27} &= -k_{21,2} \cos t_\beta + k_{22,2} \sin t_\beta \\ p_{28} &= k_{23,1} - k_{23,2} - (k_{21,2} \sin t_\beta + k_{22,2} \cos t_\beta)p_{12} \end{aligned}$$

Then, use the identity $\cos^2 \beta' + \sin^2 \beta' = 1$ to solve for $\cos \beta'$ from Eq. (8) and substitute $\cos \beta'$ into Eq. (9). This results in a trigonometric equation which contains only one variable α'

$$[e^2 - Q_1^2 - Q_2^2 - (p_{23}^2 + p_{27}^2)Q_3]^2 - 4Q_3(Q_1p_{23} + Q_2p_{27})^2 = 0 \quad (10)$$

in which

$$\begin{aligned} Q_1 &= p_{21} \cos \alpha' + p_{22} \sin \alpha' + p_{24} \\ Q_2 &= p_{25} \cos \alpha' + p_{26} \sin \alpha' + p_{28} \\ Q_3 &= -p_{11}^2 \sin^2 \alpha' - 2p_{11}p_{12} \sin \alpha' - p_{12}^2 + 1 \end{aligned}$$

The next step involves expanding Eq. (10), collecting $\cos \alpha'$ terms, and taking the squared-root of the resultant expression. The relation $\cos^2 \alpha' = 1 - \sin^2 \alpha'$ can be substituted to obtain an equation that contains only $\sin \alpha'$. If $\sin \alpha'$ is regarded as one variable, Eq. (10) can be called a univariate polynomial equation. Moreover, since the geometric meaning of Eq. (7) is the constraint $z_1 = z_2 = z$, we can also use z to substitute $\sin \alpha'$. This gives the following relationship:

$$\sin \alpha' = (z - k_{33,1})/s_1 \quad (11)$$

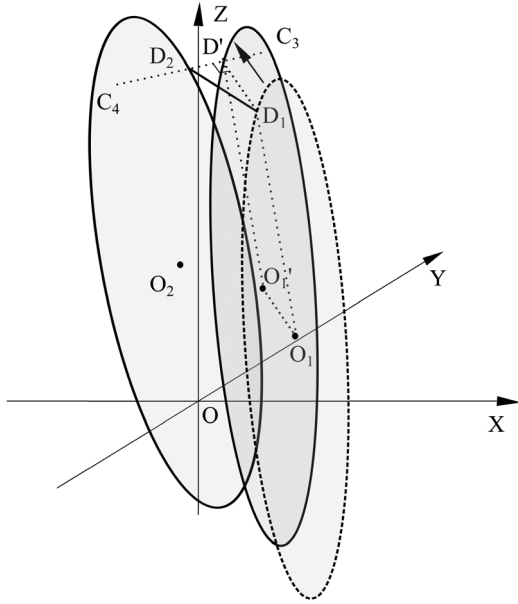


Fig. 7 For the case of a prismatic traveling plate, the constraint $\|D_1D'\| = f$ (D' is the projection of D_1 on C_3C_4) allows us to make a further simplification that involves the translation of Cir_1 from D_1 to D'

By using this relationship, Eq. (10) can be transformed into a univariate polynomial equation as a function of z

$$h_8z^8 + h_7z^7 + h_6z^6 + h_5z^5 + h_4z^4 + h_3z^3 + h_2z^2 + h_1z + h_0 = 0 \quad (12)$$

In general, for univariate polynomial equations above fourth degree, there are no analytical solutions. But they can be easily solved by numerical iteration.

2.3 Forward Kinematics for the Prismatic Traveling Plate.

As shown in Fig. 3, a prismatic traveling plate structure replaces the revolute joints with prismatic joints. Therefore, the constraints between D_1 and D_2 become the following: (a) D_1D_2 remains in the horizontal plane and (b) the distance between C_1C_2 and C_3C_4 is equal to f .

Because of the properties of these two constraints, further geometric simplification can be made. That is, move Cir_1 to Cir'_1 along vector D_1D' where D' is the projection of D_1 on C_3C_4 . As shown in Fig. 7, $\|D_1D'\| = f$. This simplification transforms the original two constraints into one: $D'D_2$ is parallel to C_3C_4 , i.e., $D'D_2 = \lambda C_3C_4$, for a coefficient λ .

By using the facts $\|D_1D'\| = f$ and $D_1D' \cdot C_3C_4 = 0$ and $C_3C_4 = -\mathbf{u}$, $D_1D' = [x_d y_d 0]^T$ can be obtained as

$$D_1D' = f \frac{\mathbf{u} \times OZ}{\|\mathbf{u} \times OZ\|}$$

Therefore, the parametric equation of Cir'_1 is given by

$$\mathbf{p}'_1 = \mathbf{p}_1 + D_1D' \quad (13)$$

where $\mathbf{p}'_1 = [x'_1 y'_1 z'_1]^T$ is the corresponding point of \mathbf{p}_1 on Cir'_1 . Since Cir_2 did not move, its parametrized equation maintains (4). Thus, the final constraint equation set for the prismatic traveling plate case is

$$\begin{cases} (x_2 - x'_1)/u_x = (y_2 - y'_1)/u_y \\ z_2 = z'_1 \end{cases} \quad (14)$$

By substituting the corresponding variables from Eqs. (4) and (13) into Eq. (14), we obtain

$$\begin{cases} k_{11,3} \cos \beta + k_{21,3} \sin \beta + k_{31,3} \\ = k_{12,3} \cos \alpha + k_{22,3} \sin \alpha + k_{32,3} \end{cases} \quad (15)$$

$$\begin{cases} k_{31,1} \cos \alpha + k_{32,1} \sin \alpha + k_{33,1} \\ = k_{31,2} \cos \beta + k_{32,2} \sin \beta + k_{33,2} \end{cases} \quad (16)$$

where $k_{pq,3}$ is the entry located at the p th row and the q th column in a new coefficient matrix \mathbf{K}_3 .

$$\mathbf{K}_3 = \begin{bmatrix} u_y k_{11,2} - u_x k_{21,2} & u_y k_{11,1} - u_x k_{21,1} \\ u_y k_{12,2} - u_x k_{22,2} & u_y k_{12,1} - u_x k_{22,1} \\ u_y k_{13,2} - u_x k_{23,2} & u_y(k_{13,1} + x_d) - u_x(k_{23,1} + y_d) \end{bmatrix}$$

Using the same substitution method as in Eq. (7), Eq. (15) can be simplified to

$$p_{31} \cos \beta' + p_{32} \sin \beta' = p_{33} \cos \alpha' + p_{34} \sin \alpha' + p_{35} \quad (17)$$

where

$$p_{31} = k_{11,3} \cos t_\beta - k_{21,3} \sin t_\beta$$

$$p_{32} = k_{11,3} \sin t_\beta + k_{21,3} \cos t_\beta$$

$$p_{33} = k_{12,3} \cos t_\alpha - k_{22,3} \sin t_\alpha$$

$$p_{34} = k_{12,3} \sin t_\alpha + k_{22,3} \cos t_\alpha$$

$$p_{35} = k_{32,3} - k_{31,3}$$

Note that Eq. (16) is the same as Eq. (5). Thus, we can use relationship (8) directly to substitute β' in Eq. (17). This yields a trigonometric equation which contains only one variable α'

$$\begin{aligned} & p_{31}^2 [1 - (p_{11} \sin \alpha' + p_{12})^2] \\ & = [p_{33} \cos \alpha' + (p_{34} - p_{32} p_{11}) \sin \alpha' + p_{35} - p_{12} p_{32}]^2 \end{aligned} \quad (18)$$

The same strategy as in Sec. 2.2 can be used to obtain a univariate polynomial equation with unknown z

$$t_4 z^4 + t_3 z^3 + t_2 z^2 + t_1 z + t_0 = 0 \quad (19)$$

The roots of this quartic equation can be computed using the quartic root formulas [25], although numerical solutions may be more convenient.

3 Discussion About the Real Roots

As shown earlier, the forward kinematic equations for H4 robots with articulated traveling plate can be transformed into an eighth degree univariate polynomial equation, while H4 robots with prismatic traveling plate have a fourth degree univariate polynomial equation. Algebraically, an eighth degree real coefficient univariate polynomial has exactly eight roots in the complex domain and all complex roots must appear in conjugacy. This means the number of complex roots cannot be odd. However, due to the multiplicity, the actual nonrepeated real roots could still be odd numbers (for instance, two repeated real roots are actually one nonrepeated root). So in theory, there could exist up to eight real roots for the general H4 mechanism. This becomes clear if we consider the physical meaning of Eq. (12). This equation can be obtained by constraining the length and direction of D_1D_2 . This means that each nonrepeated real root of Eq. (12) corresponds to one distinct D_1D_2 . Therefore, we can find the number of real roots by looking at the number of distinct D_1D_2 between Cir_1 and Cir_2 . Vice versa, we can investigate the possible configurations of H4

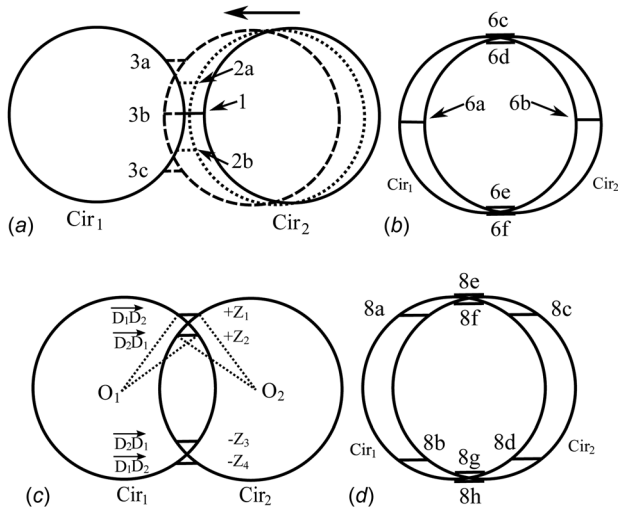


Fig. 8 The existence of nonrepeated real root number is illustrated by intentionally letting Cir_1 and Cir_2 be in the same plane, which is not very hard to find in practice. In these figures, the line segments connecting two circles are the compatible D_1D_2 s with Eq. (12). The unillustrated five root case and seven root case can be achieved from the six root case by slightly enlarging or shrinking Cir_2 so that the mid root on the right side disappears or splits into two. A number and an alphabetical letter are used to label a specific root configuration: (a) As Cir_2 moves left, the real root emerges from null to three, (b) six real roots case, (c) if we keep moving Cir_2 left from the three roots case, the mid root bifurcates and generates the four real roots case. This figure also shows different D_1D_2 s and their corresponding z coordinate, and (d) eight real roots case.

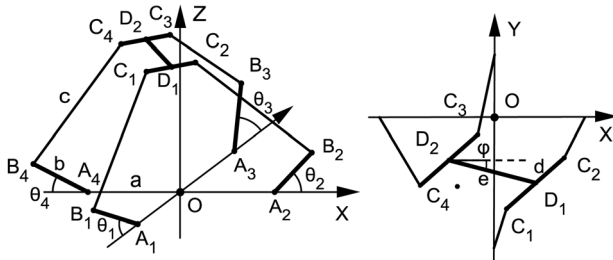


Fig. 9 The design parameters of a H4 robot with articulated traveling plate (the right figure shows the top view with the parameters of the traveling plate)

by looking at the nonrepeated real roots. Figure 8 shows the existence of nonrepeated real root number.

Note that Fig. 8 only shows the existence of nonrepeated number of real roots for the general H4 mechanism. For a specific H4 robot, the number of real roots depends on the actual positions of Cir_1 and Cir_2 which turns out to be very hard to analyze in advance. However, we can still investigate this by numerically checking a regular 4DOF grid in the workspace. Section 3.1 is an example of the H4 robot in Fig. 2. This model is used to investigate the root number. A specific point is also chosen (who has four real roots) in joint space to show the corresponding configurations for each real root.

3.1 The Nonrepeated Real Root of the H4 Robot With an Articulated Traveling Plate. Figure 9 shows the design parameters of a H4 robot with articulated traveling plate and the global coordinate system (O, X, Y, Z). This figure intends to capture the kinematic configurations in Fig. 2. The used design parameters in this paper are base radius $a = 400$ mm, arm length $b = 300$ mm,

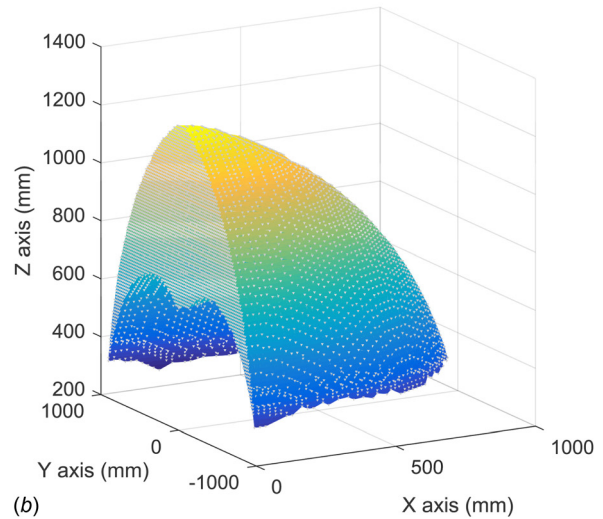
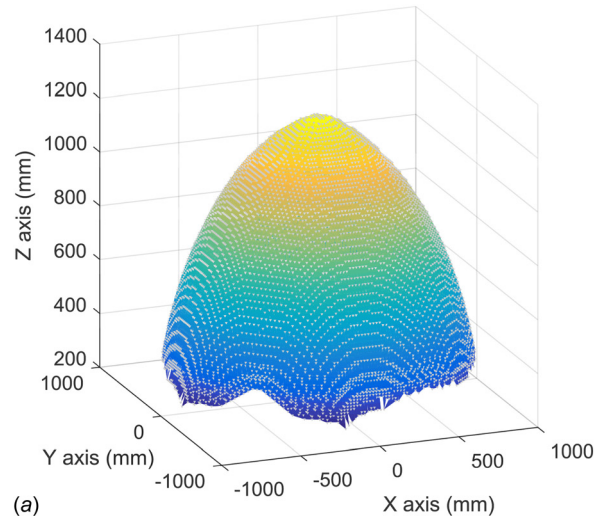


Fig. 10 Workspace of the H4 robot in Fig. 2: position plot of the central bar: (a) three-dimensional view of the workspace of the H4 robot in Fig. 2 and (b) section view of the workspace of the H4 robot in Fig. 2 (section plane $x = 0$)

forearm length $c = 1000$ mm, lateral bar length $d = 100$ mm, and central bar length $e = 100$ mm.

To count the real roots in the workspace, we need to calculate the workspace first. This can be done by checking a 4DOF grid $[-1000, 1000] \times [-1000, 1000] \times [200, 1000] \times [-\pi/4, 3\pi/4]$ by the inverse kinematics (the inverse kinematics algorithm for H4 can be found in Ref. [23]). The workspace of the H4 robot in Fig. 2 is shown in Fig. 10. During this process, all joint angles whose corresponding point is in the workspace were recorded. These joint angles were then used to compute the GFK and count the number of real roots.

Figure 11 shows the spatial distribution of different real roots. It is worth to note that zero real roots are not needed since only the joint angles from the inverse kinematics are chosen. Therefore, there is at least one real root for all points. In addition, one, three, five, seven, or eight nonrepeated real roots were not found either. This may be attributed to the fact that our grid was not sufficiently fine. But a more important reason is that these root cases only appear in specific mechanisms with very special kinematic configurations (referring to Fig. 8).

However, we did find several points with six nonrepeated real roots, as shown in Fig. 11(c). These points appear in symmetry. Another interesting observation is the distributions of the two real

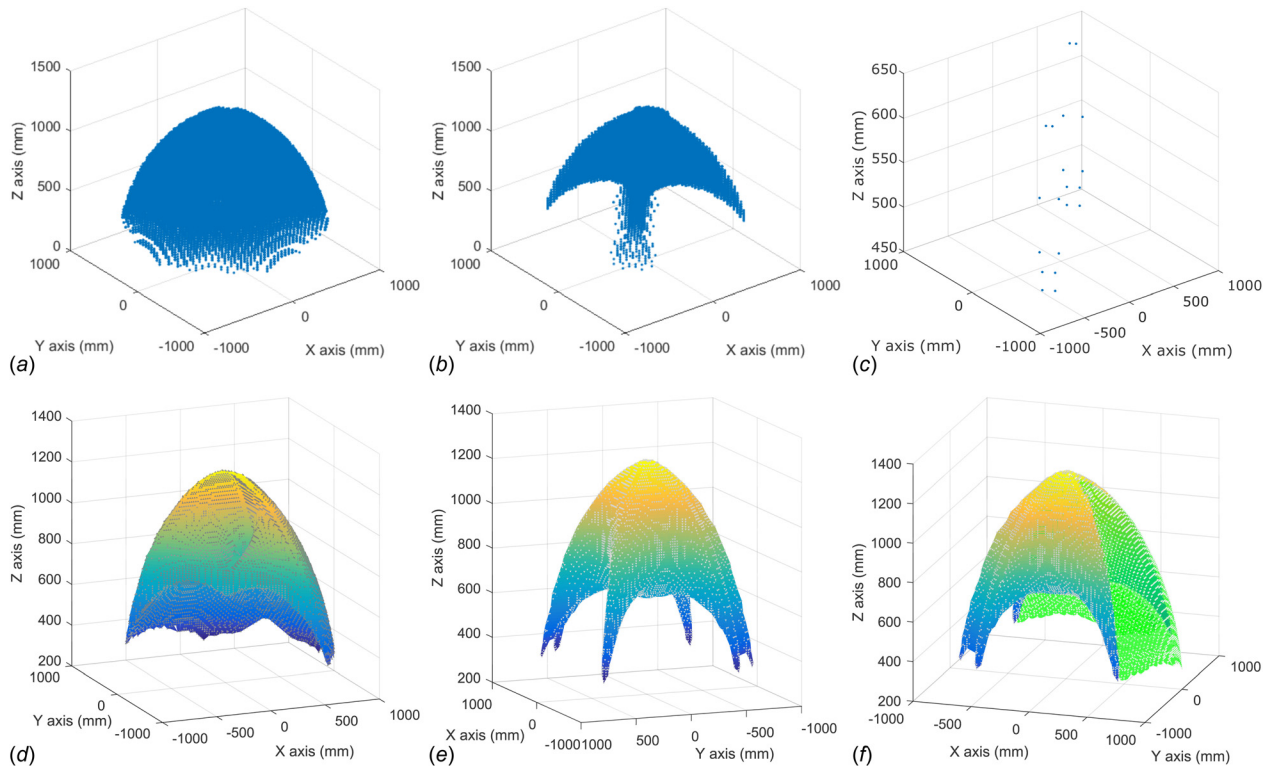


Fig. 11 Distribution of points with different nonrepeated real roots and their enveloping solid: (a) distribution of points with two nonrepeated real roots, (b) distribution of points with four nonrepeated real roots, (c) distribution of points with six nonrepeated real roots, (d) section view (section plane $y = -x$) of the enveloping solid of (a). Note that this section view shows a hollow inside (a), (e) enveloping solid of (b), and (f) joint view for (d) and (e). The enveloping solid in (d) was changed to transparent green in order to get a better view.

roots case and the four real roots case. From Fig. 11(f), these two cases constitute most of the workspace but they are not clearly separated by a boundary. Instead, there exists some overlapping areas. This observation implies that there exist some continuous

regions (this simply connected manifold in mathematics is called component) in the workspace that any point in these regions has only two nonrepeated real roots (or four for other components). Since nonrepeated real root means the valid geometric configurations of the robot, this statement is equivalent to say that there exist some continuous regions in the workspace such that the robot has only two (or four for other components) possible geometric configurations. Further investigations show that for the H4 robot in Fig. 2, the two configurations in the two root component are the two cases shown in Figs. 12(a) and 12(c).

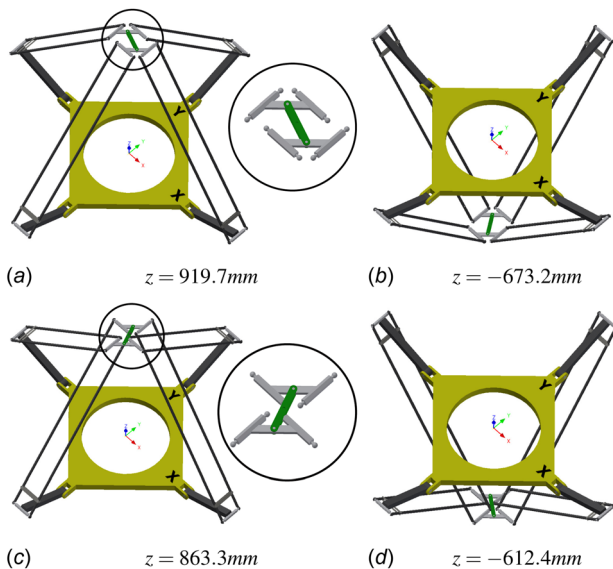


Fig. 12 Configurations of the four real roots. Note that the inside planar bar near the traveling plate in the parallelogram was set transparent to get a clear view of each configuration. The traveling plate in subfigures (b) and (d) has a similar configuration as in (a) and (c): (a) $z = 919.7\text{mm}$, (b) $z = -673.2\text{mm}$, (c) $z = 863.3\text{mm}$, and (d) $z = -612.4\text{mm}$.

3.2 Four Configurations for a Specific Point of the H4 Robot.

Given $\mathbf{q} = [\pi/6 \ \pi/7 \ \pi/8 \ \pi/9]^T$, the univariate polynomial equation of z becomes

$$-3.366 \times 10^{-5}z^8 - 4.503 \times 10^{-3}z^7 - 4.073 \times 10^4z^6 + 4.884 \times 10^6z^5 - 1.276 \times 10^{13}z^4 + 6.379 \times 10^{15}z^3 + 1.390 \times 10^{19}z^2 - 3.666 \times 10^{21}z - 4.195 \times 10^{24} = 0$$

Its eight roots are

$$[2231 + 24880i, 2231 - 24880i, -2547 + 24560i, -2547 - 24560i, 919.7, 863.3, -673.2, -612.4]$$

As these roots are the possible z coordinates of the traveling plate, only the four real ones are valid in geometry. Among these four real roots, the negative two represent the cases that the traveling plate is above the base and the positive two represent below the base, as shown in Fig. 12. The difference between the two positive roots lies in the opposite directions of $\mathbf{D}_1\mathbf{D}_2$. That is because the direction of $\mathbf{D}_1\mathbf{D}_2$ in Eqs. (5) and (6) was not constrained.

Obviously, the right direction of $\mathbf{D}_1\mathbf{D}_2$ should ensure that the fore-arms do not collide. In practice, this can be done by specifying the range of the rotation angle of the central bar.

In general, a good procedure to pick the correct solution of the GFK is restricting all the possible solutions in the workspace at first (the workspace can be obtained by inverse kinematics beforehand). Then for those incorrect solutions in the workspace, the rotation angle limit of the central bar (for instance, from -45 deg to 135 deg) can be used to eliminate them.

3.3 Numerical Robustness of the Geometric Forward Kinematics and Failure Analysis. For parallel robots, a practical problem of kinematic analysis is the robustness of the algorithm. The computation may fail near the singularities. Therefore, in this section, we performed a numerical check to see if the GFK algorithm works for every point in the workspace. This is done in two main steps. First, the GFK is checked for at least one real root for all workspace points and whether it is capable of picking the right solution when there are more than one real roots. The second step involves comparing the workspace points with the points computed by GFK. The error between these two points indicates the numerical accuracy of our algorithm. Note that this error also contains the inverse kinematics error since we used the inverse kinematics to map the workspace point to the joint space point before applying GFK. However, for parallel mechanisms, the inverse kinematics can be assumed accurately and reliably due to its simplicity. So, this error is still reflected in the GFK's precision. We use MathWorks MATLAB (the default computation precision is 16 digits numbers) to perform the computation and use the same grid as in Sec. 3.1.

From Sec. 3.1, no point with zero real root was found in the workspace. Thus, for the first part, we only need to check if the GFK algorithm can pick the correct solution. This actually can be done by the second part if we consider a big error as a wrong pick.

The numerical experiment shows that the proposed algorithm is capable of computing all the available solutions. However, we did detect some failure points (4134 failure points out of 344,220 points) for which the program could not pick the right solution. Further investigation shows that this failure is caused by the selection subroutine. Since we only restricted the range of ϕ angle, the selection subroutine is not able to eliminate the plausible solutions who also satisfy this condition. For instance, when $\mathbf{q} = [-1.329 - 0.324 \ 0.749 - 0.0183]^T$ rad, Eq. (12) has two very close positive real roots $z_1 = 688.9$ and $z_2 = 686.8$. The two corresponding solutions in the workspace are $X_1 = [20.41 \text{ mm} - 265.3 \text{ mm} \ 688.9 \text{ mm} - 0.5236 \text{ rad}]^T$ and $X_2 = [18.06 \text{ mm} - 260.5 \text{ mm} \ 686.8 \text{ mm} - 0.6662 \text{ rad}]^T$.

It is observable that both these close solutions satisfy the constraint equation as well as the restriction of $\mathbf{D}_1\mathbf{D}_2$ rotational angle. In fact, these two positions are two valid solutions for the real robot. Therefore, for these points, restricting the rotational angle of the central bar or restricting operation range of other moving parts cannot eliminate the plausible solution. The only way to eliminate them is to consider the current position of the robot since a physical object cannot change its position discontinuously. The right position of this object after a small amount of time should be close to its current position. Moreover, since we stated in Sec. 3 that every distinct real root corresponds to a distinct $\mathbf{D}_1\mathbf{D}_2$, the two close solutions actually correspond to a specific configuration of Cir_1 and Cir_2 such that the two distinct $\mathbf{D}_1\mathbf{D}_2$ are close to each other. This happens when the two circles Cir_1 and Cir_2 move close to each other so that the two solutions merge into one solution (as shown in Fig. 8(a)).

For those successfully picked points, the maximum error norm is 9.8775×10^{-5} (due to the angle component for the workspace points, this norm does not have a physical unit) and the mean error norm is 4.5779×10^{-9} . This shows that our algorithm exhibits good accuracy.

Note that we used a larger ϕ range (180 deg, compared with the practically used range 90 deg) to fully explore the root properties. If we restrict the ϕ range to 90 deg, it turns out that there is only one valid solution inside the workspace, which is consistent with the result in Ref. [19].

4 Conclusion

In this paper, a new geometry-based method to obtain the closed-form forward kinematics solution of 4DOF H4 parallel robots is developed. The result shows that the forward kinematics of the H4 robots with articulated traveling plate yields an eighth degree univariate polynomial equation, as well as the prismatic traveling plate case yields a simpler fourth degree univariate polynomial equation. For both situations, this method has a more simplified derivation and clearer physical meanings than the earlier reported results. Thanks to its clear physical meaning, an intensive discussion about the solutions was possible. The investigations show that a general H4 robot can have up to eight nonrepeated real solutions for its forward kinematics. For a specific configuration of H4, the nonrepeated real root number could be only two, four, or six. The numerical analysis shows that GFK can successfully find all the solutions with good accuracy although there exist some failure points that require more historical information to avoid.

Nomenclature

- a = radius of the robot base (distance between O and A_i)
- A_i = position of the actuation joint of chain i
- b = arm length (distance between A_i and B_i)
- B_i = elbow point of chain i
- B'_i = new position of B_i after translation
- C_i = endpoint of the lateral bar on chain i
- c = forearm length (distance between B_i and C_i)
- Cir_j = the parametrized circle centering at O_j with a radius of r_j and a normal vector \mathbf{n}_j
- d = lateral bar length (distance between C_1 and C_2)
- D_1 = midpoint of the lateral bar C_1C_2
- D_2 = midpoint of the lateral bar C_4C_3
- e = central bar length (distance between D_1 and D_2)
- E = midpoint of the central bar D_1D_2
- f = distance between the two lateral bars for the prismatic traveling plate
- i = index of each chain ($i = 1, \dots, 4$)
- j = index of the two parametrized circles ($j = 1, 2$)
- $k_{pq,r}$ = entry of matrix \mathbf{K}_r in the p th row and the q th column
- \mathbf{K}_j = coefficient matrix for the parametrized equation of Cir_j
- \mathbf{K}_3 = coefficient matrix for the constraint equation set of the prismatic traveling plate
- \mathbf{n}_1 = vector $\mathbf{B}'_1\mathbf{B}'_2$ whose three components are $n_{x,1}$, $n_{y,1}$, and $n_{z,1}$
- \mathbf{n}_2 = vector $\mathbf{B}'_4\mathbf{B}'_3$ whose three components are $n_{x,2}$, $n_{y,2}$, and $n_{z,2}$
- O_1 = midpoint of $B'_1B'_2$ whose three components are $o_{x,1}$, $o_{y,1}$, and $o_{z,1}$
- O_2 = midpoint of $B'_3B'_4$ whose three components are $o_{x,2}$, $o_{y,2}$, and $o_{z,2}$
- \mathbf{p}_j = an arbitrary point on Cir_j whose three components are x_j , y_j , and z_j
- $\mathbf{q} = [q_1, q_2, q_3, q_4]^T$ = actuated joint positions
- \mathbf{u} = vector $\mathbf{C}_1\mathbf{C}_2$ whose three components are u_x , u_y , and u_z

$X = [x, y, z, \phi]^T$ = task space coordinates (position of point E ;
 motion angle of the central bar)
 α = parameterized variable for Cir_1
 β = parameterized variable for Cir_2

References

- [1] Merlet, J.-P., 2006, *Parallel Robots*, Springer, Dordrecht, The Netherlands.
- [2] Han, X., and Zhang, J., 2013, "A Method to Get the Forward Kinematics of Parallel Kinematics Mechanisms Based on the Fixed Point Iteration," *Advanced Materials Research* (Materials Processing and Manufacturing III), Vol. 753–755, Trans Tech Publications Inc, Zürich, Switzerland, pp. 2949–2953.
- [3] Cardona, M., 2015, "A New Approach for the Forward Kinematics of General Stewart-Gough Platforms," IEEE 35th Central American and Panama Convention (Concapan XXXV), Tegucigalpa, Honduras, Nov. 11–13, pp. 1–16.
- [4] Lv, W., Tao, L., and Hu, Y., 2017, "On the Real-Time Calculation of the Forward Kinematics of a Suspended Cable-Driven Parallel Mechanism With 6-Degree-of-Freedom Wave Compensation," *Adv. Mech. Eng.*, **9**(6), pp. 1–17.
- [5] Merlet, J., 2004, "Solving the Forward Kinematics of a Gough-Type Parallel Manipulator With Interval Analysis," *Int. J. Rob. Res.*, **23**(3), pp. 221–235.
- [6] Innocenti, C., 2001, "Forward Kinematics in Polynomial Form of the General Stewart Platform," *ASME J. Mech. Des.*, **123**(2), pp. 254–260.
- [7] Raghavan, M., 1993, "The Stewart Platform of General Geometry Has 40 Configurations," *ASME J. Mech. Des.*, **115**(2), pp. 277–282.
- [8] Lee, T., and Shim, J., 2001, "Forward Kinematics of the General 6-6 Stewart Platform Using Algebraic Elimination," *Mech. Mach. Theory*, **36**(9), pp. 1073–1085.
- [9] Huang, X., Liao, Q., and Wei, S., 2010, "Closed-Form Forward Kinematics for a Symmetrical 6-6 Stewart Platform Using Algebraic Elimination," *Mech. Mach. Theory*, **45**(2), pp. 327–334.
- [10] Zoppi, M., Zlatanov, D., and Gosselin, C., 2005, "Analytical Kinematics Models and Special Geometries of a Class of 4-DOF Parallel Mechanisms," *IEEE Trans. Rob.*, **21**(6), pp. 1046–1055.
- [11] Sterheim, F., 1987, "Computation of the Direct and Inverse Geometric-Models of the Delta-4 Parallel Robot," *Robotersysteme*, **3**(4), pp. 199–203.
- [12] Nam, Y.-J., and Park, M.-K., 2006, "Forward Kinematics of Casing Oscillator," *IEEE-ASME Trans. Mechatronics*, **11**(5), pp. 644–647.
- [13] Song, S., and Kwon, D., 2002, "Geometric Formulation Approach for Determining the Actual Solution of the Forward Kinematics of 6-DOF Parallel Manipulators," IEEE/RSJ International Conference on Intelligent Robots and Systems, Lausanne, Switzerland, Sept. 30–Oct. 4, pp. 1930–1935.
- [14] Gallardo-Alvarado, J., Rico-Martinez, J. M., and Alici, G., 2006, "Kinematics and Singularity Analyses of a 4-DOF Parallel Manipulator Using Screw Theory," *Mech. Mach. Theory*, **41**(9), pp. 1048–1061.
- [15] Muller, A., and Maisser, P., 2003, "A Lie-Group Formulation of Kinematics and Dynamics of Constrained MBS and Its Application to Analytical Mechanics," *Multibody Syst. Dyn.*, **9**(4), pp. 311–352.
- [16] Yang, X., Wu, H., Li, Y., and Chen, B., 2017, "A Dual Quaternion Solution to the Forward Kinematics of a Class of Six-DOF Parallel Robots With Full or Reductant Actuation," *Mech. Mach. Theory*, **107**, pp. 27–36.
- [17] Company, O., Marquet, F., and Pierrot, F., 2003, "A New High-Speed 4-DOF Parallel Robot Synthesis and Modeling Issues," *IEEE Trans. Rob. Autom.*, **19**(3), pp. 411–420.
- [18] Choi, H.-B., Konno, A., and Uchiyama, M., 2009, "Closed-Form Forward Kinematics Solutions of a 4-DOF Parallel Robot," *Int. J. Control Autom. Syst.*, **7**(5), pp. 858–864.
- [19] Pierrot, F., Nabat, V., Company, O., Krut, S., and Poignet, P., 2009, "Optimal Design of a 4-DOF Parallel Manipulator: From Academia to Industry," *IEEE Trans. Rob.*, **25**(2), pp. 213–224.
- [20] Krut, S., Company, O., Benoit, M., Ota, H., and Pierrot, F., 2003, "I4: A New Parallel Mechanism for Scara Motions," IEEE International Conference on Robotics and Automation, Taipei, Taiwan, Sept. 14–19, pp. 1875–1880.
- [21] Krut, S., Nabat, V., Company, O., and Pierrot, F., 2004, "A High-Speed Parallel Robot for Scara Motions," IEEE International Conference on Robotics and Automation (IRCA), New Orleans, LA, Apr. 26–May 1, pp. 4109–4115.
- [22] Krut, S., Company, O., Nabat, V., and Pierrot, F., 2006, "Heli4: A Parallel Robot for Scara Motions With a Very Compact Traveling Plate and a Symmetrical Design," IEEE/RSJ International Conference on Intelligent Robots and Systems (IROS), Beijing, China, Oct. 9–15, pp. 1656–1661.
- [23] Pierrot, F., and Company, O., 1999, "H4: A New Family of 4-DOF Parallel Robots," IEEE/ASME International Conference on Advanced Intelligent Mechatronics, Atlanta, GA, Sept. 19–23, pp. 508–513.
- [24] Company, O., Krut, S., and Pierrot, F., 2006, "Internal Singularity Analysis of a Class of Lower Mobility Parallel Manipulators With Articulated Traveling Plate," *IEEE Trans. Rob.*, **22**(1), pp. 1–11.
- [25] Shmakov, S., 2011, "A Universal Method of Solving Quartic Equations," *Int. J. Pure Appl. Math.*, **71**(2), pp. 251–259.